Apparent Temperature of Mercury, Mars, Saturn and Venus at X Band

April 6, 2004

Glen Langston, Jim Braatz, Frank Ghigo, Ron Maddalena,

Toney Minter and Karen O'Neal

Abstract

This note presents observations with the GBT in the frequency range 8 to 10 GHz (X band receiver). Efficiency and pointing test results are presented for observations of Mercury, Venus, Mars and Saturn. Spectral line band scans on the planets shows that the receiver appears to be functioning well at all frequencies between 8 and 10 GHz. At 9 GHz, the aperture efficiency, η_A is = 0.64 ±0.05 at 80 degrees elevation, based on observations of 3C48. We estimate the GBT beam efficiency, η_B = 0.87±0.07 and confirm this value with observations of the planets. The observational technique applied here is important at higher frequencies where the GBT efficiency is more uncertain.

1 Introduction

GBT Observations with the 8 to 10 GHz receiver were made on July 5, 2003 using the Digital Continuum Receiver (DCR) and the Auto-Correlation Spectrometer (ACS). These observations were made to check the broad band capabilities of the ACS, and also test the gain stability of the IF rack, optical fiber drivers, optical fiber receivers in the equipment room, the converter rack and associated local oscillators and the internal gain of the ACS.

The data were obtained using the GBT Observe program, performing "Peak" procedures to find the pointing offsets. All spectral line observations were made using the "OffOn" procedure.

Data were assigned to test observations for project "TSDSS_01". A selection of the observing scan log is given in Table 1. The computed distances of the planets on the date of observations are given in Table 2. The distance from Green Bank to the planets were accurately estimated using the JPL solar system ephemeris.

Note that the small angular separation between the Sun and Mercury Venus and Saturn limits the accuracy of the planet temperature determination. The spectra were analyzed using `aips++` and glish scripts (`tip.g, GOpoint.g`) written by Jim Braatz.

2 GBT Beam Measurements

Based on observations of compact radio source 3C48, we find the GBT FWHM beam width at 9 GHz (λ = 3.33 cm) is 1.408 ±0.003 arc-min. In real time the peaks were examined using `iards` to look at the pointing offsets, before starting the spectral line observations.

We assume the FWHM beam width scales simply with wavelength, and for the purposes of brightness temperature calculations, the beam width is given by

$$\theta_A(\lambda) = \frac{1.408 \pm 0.003'}{3.33} \quad \frac{\lambda}{1\ cm} = 0.423 \pm 0.001' \frac{\lambda}{1\ cm},$$

where λ is the wavelength in cm.

Following Baars (1973) we use the main beam area, Ω_m, formula below,

$$\Omega_m = 1.133\ \theta_A^2.$$

At 9 GHz, the GBT beam area is 2.246 arc-min^2 = 1.900×10^{-7} sr.

2.1 ACS Setup

For the first hour of the tests, the ACS was set up in the A1 800 MHz bandwidth, three level, dual polarization mode, producing 2048 lags per spectrum. The planets Mars and Venus were observed in this mode, stepping by 600 MHz across the receiver band, at 8400, 9000 and 9600 MHz center frequencies, covering the frequency range 8000 to 1000 GHz, with 200 MHz overlap between spectra. The Cal On/Off switching cycle of 1 Hz was selected, using external blanking and external Cal On/Off signals. The switching signal selector was configured to route the internally generated ACS switching signals back into the ACS. The integration time of 10 seconds was selected. Scan durations were usually 60 seconds.

During the second hour, the ACS was set up in the A1,B1,C1,D1 800 MHz mode simultaneously observing 4 center frequencies, 8400, 9000, 9600 and 10200 MHz. Each spectrum was 800 MHz wide, producing 2048 lags per band.

2.2 Tipping Curves

No observations of the system temperature versus elevation angle were made during this observing session, since the atmospheric attenuation was expected to be small in good weather. Observations at other times show that a "typical" atmospheric attenuation value of $\tau = 0.01$ can be assumed in good weather, when observing at 9 GHz.

Figure 1 shows an example a fit of attenuation to an observation at 9 GHz. In this case, the observations are well fit by attenuation, $\tau = 0.008 \pm 0.001$. Other observations in less excellent weather showed $tau < 0.014$. For the remainder of this document $\tau = 0.01$ is assumed.

Table 3 lists the atmospheric attenuation factor, $exp(tau/sin(El))$ for the elevation angles at the time of observation of the planets.

3 3C48

Compact radio source 3C48 is used as a calibration reference for radio wavelength observations in the frequency range 1.4 to 15 GHz. At 9 GHz, the Ott *et al.*(1994) fit yields a flux density of 3.112 ± 0.244 for 3C48. Note that the uncertainty in the 3C48 flux density dominates the our uncertainty in the measurement of the GBT efficiency.

For bright radio sources like 3C48, the dominant observational uncertainty is the uncertainty in the calibration of the effective temperature of the noise diode values. For 3C48 at 9 GHz we observe $T_R = 5.509 \pm 0.009$ K and $T_L = 5.659 \pm 0.012$ K. Notice that the RMS noise in the measurements for the two polarizations is much smaller than the difference between the two values. We assuming little circular polarization for source 3C48 and the planets. We adopt the average left and right circular polarization temperature for antenna temperature and take the difference between the temperature of the average and the difference of the polarizations as an estimate of the error in the antenna temperature (Ie. $T_A = \frac{1}{2}[(T_R + T_L) \pm (T_R - T_L)] = 5.584 \pm 0.075$).

Adopting the notation and numerical values of Ghigo et al (2001), the source flux density is

$$S = \frac{2kT_A}{\eta_A A_g}$$

where k is Boltzman's constant, and A_g is the geometric area of the GBT, 7854 m^2. Substituting the numerical values for k and the 3C48 observations, we find

$$\eta_A = \frac{2761 \times 5.584 \pm 0.075}{3.112 \pm 0.244 \times 7854} = \frac{1}{2.845} \times \frac{5.584 \pm 0.075}{3.112 \pm 0.244} = 0.64 \pm 0.05,$$

where the major contribution to the uncertainty in η_A is the uncertainty in the flux density of 3C48.

3.1 Planet Data Analysis

The four primary conversion factors from observed antenna temperature are summarized below.

η_A Aperture efficiency, determined by observations of compact extra-galactic radio sources.

BeamDilution The ratio of the telescope beam area to the angular area of the planet on the date of observation. This is a large factor if the angular size of the planet is much smaller than the telescope beam.

DiskFactor The convolution function of a uniform temperature disk with a Gaussian beam. This is a small factor if the angular size of the planet is much smaller than the telescope beam.

τ Atmospheric attenuation. At 9 GHz in good weather the atmospheric attenuation factor is small, less than 3 percent for these observations.

The beam dilution factor is the ratio of the areas of the planet and the GBT beam area at the frequency of observation. The planet angular area is simply $\pi\theta_S^2/4$, where θ_S is the angular diameter of the planet. Table 2 lists the angular sizes of the planets on the date of observations.

Following Baars (1973) equation 12, we correct the antenna response for the the disk shaped projected surface of the planet using

$$K = \frac{x^2}{1 - exp(-x^2)}$$

where $x = \theta_S/1.2\ \theta_A$. Table 3 lists the dilution and disk factors on the date of observations.

The conversion from antenna temperature, T_A, to brightness temperature, T_B requires an estimate of the beam efficiency η_B. We assume the GBT radiation efficiency, η_R, is 0.99 at 9 GHz and estimate η_B using equation 10 of Baars 1973:

$$\eta_B = \frac{\eta_A \Omega_m A_g}{\eta_R \lambda^2} = \frac{0.64{\pm}0.05 \times 1.9 \times 10^{-7} \times 7854}{0.99 \times 0.0333^2} = 0.87{\pm}0.07.$$

The computation of the physical temperature of the planets was performed using `aips++ dish` glish scripts. An example script is included in appendix A.

3.2 Mars

The 9 GHz band average antenna temperature towards Mars was 5.447 ±0.075 K. On July 5, 2003, Mars was 8.02×10^7 km from Green Bank, and the angular diameter of Mars was 0.290 arc-min. The beam dilution, disk and atmospheric attenuation factors are given in Table 3. Using $\eta_B = 0.87{\pm}0.07$ yields $T_{B,Mars} = 221{\pm}16$ K.

Figure 6 shows the antenna temperature of Mars, calibrated by measurement of the intensity of the noise diode values, which are toggled on and off at a 1 Hz rate during the scans. Three scans are shown in this figure, one centered at 8400 MHz, one at 9000 MHz and the third at 9600 MHz. Figure 7 shows the same data as figure 6, zoomed on the average antenna temperature of Mars. Notice the undulations in the band pass spectrum which are due to the resonances in the GBT feed and receiver system. There is a very strong line at 8400 MHz in the Mars spectrum due to down link data from satellites at Mars. This signal is much much stronger in the Right circular polarization.

The orbit of Mars is eccentric, $e = 0.093$, and the physical temperature of Mars is dependent on the distance from the Sun at the time of observation according to the function below (de Pater 1990):

$$T_{B,Mars,Ave}(\nu) = T_{B,Mars}(\nu)\sqrt{\frac{r}{r_M}}$$

where r_M is the mean solar distance, 1.524 AU, and $T_{Mars,Ave}(\nu)$ is the average temperature of Mars. At the date of these observations, r=1.402 AU, so the correction factor from observed brightness temperature to average temperature is 0.959, yielding $T_{B,Mars,Ave}(9GHz) = 212{\pm}15$ K. This value is higher than the value reported by Rudy (1987) at 2 cm, 193 ±10 K, averaged over the whole Mars disk and corrected to the average temperature at the mean Mars orbital radius.

Figure 9 shows the brightness temperature of Mars, calibrated by calculating $\eta_B(\nu)$ for each spectral channel, using the observations of 3C48 at the same frequency. The glish scripts in the

appendix show the details of this calibration procedure. Notice the narrow features due to the GBT feed and receiver are removed by this calibration process. Figure 10 shows the same data as figure 9, centered on the average brightness temperature of Mars. The scans centered at 9000 and 9600 MHz show good temperature agreement, while the scan at 8400 MHz center frequency has a different average brightness temperature where overlapping with the 9000 MHz scan. This may be due to gain compression due to the strong signal at 8400 GHz.

3.3 Mercury

The observations of Mercury were made when the planet was only a few degrees from the Sun and the spectral baselines show significant undulations. The 9 GHz average antenna temperature was 0.59 ±0.18 K. On July 5, 2003, Mercury was 1.988×10^8 km from Green Bank. and the angular diameter of Mercury was 0.0841 arc-min. The beam dilution, disk and atmospheric attenuation factors are given in table 3. Using $\eta_B = 0.87 \pm 0.07$ yields $T_{B,Mercury} = 282 \pm 85$ K. For Mercury the uncertainty in the estimate of the effective brightness temperature is dominated by undulations in the spectral baselines. The accuracy of these observations could be improved by observations of Mercury when its angular distance from the Sun was greater. Figure 6 shows the undulating T_B spectrum of Mercury. This figure shows the good agreement in the calibration of the overlapping frequency range of the four spectra. The undulations of the T_B versus frequency happen to bring the Mercury brightness temperature to a reasonable at 9 GHz, the reference frequency for this study. These observations should be repeated when Mercury is further from the Sun.

VLA observations at 6 cm by Burns *et al.* 1987 show the brightness temperature of Mercury is significantly greater on the Sun-lit side of Mercury. Klein (1970) finds the Mercury effective temperature ranging between 300 and 440 K for the night and day sides respectively.

3.4 Saturn

The 9 GHz average antenna temperature towards Saturn was 5.256 ±0.062 K. On July 5, 2003, Saturn was 1.501×10^9 km from Green Bank, and the angular diameter of Saturn was 0.2667 arc-min. The beam dilution, disk and atmospheric attenuation factors are given in table 3. Using $\eta_B = 0.87 \pm 0.07$ yields $T_{B,Saturn} = 151.8 \pm 12$ K.

The measurement uncertainty in the estimated brightness temperature is dominated by uncertainty in calibration of the GBT. The observed effective temperature is consistent with the data of Briggs and Sackett (1989), 165 ±15 K, that is reported in de Pater (1990).

The broad, $\sim$ 200 MHz, undulations in the band spectrum of Saturn near 9800 and 10100 MHz also appear in the Venus spectra (below), and are likely due to a problem with input spectrometer power during the observation of 3C48. The 3C48 observation at 10 GHz is used to calibrate the observations of Venus and Saturn.

3.5 Venus

The 9 GHz average antenna temperature was 5.256 ±0.062 K. On July 5, 2003, Venus was 2.517×10^8 km from Green Bank, and the angular diameter of Venus was 0.1653 arc-min. The beam dilution, disk and atmospheric attenuation factors are given in table 3. Using $\eta_B = 0.87 \pm 0.07$ yields $T_{B,Venus} = 648 \pm 48$ K.

The measurement uncertainty in the estimated brightness temperature is dominated by uncertainty in calibration of the GBT. Pettengill *et al.* 1988 measured 636 ±28 K for the disk averaged brightness temperature of Venus.

Figure 10 shows the brightness temperature of Venus, calibrated by calculating $\eta_B(\nu)$ for each spectral channel, using the observations of 3C48 at the same frequency. Notice the narrow features due to the GBT feed and receiver are removed by this calibration process. Figure 11 shows the same data as figure 10, centered on the average brightness temperature of Venus. Notice the very high brightness temperature of Venus, due to the Green house effect. At lower frequencies the atmosphere is more transparent, so that the radio wavelength observations reach deep in the Venus atmosphere, to hotter regions, where the effective temperature is greater.

While there is good agreement between frequency bands for the Venus observations, clearly there is a discrepancy of approximately 20 K where the 800 MHz spectral bands overlap. This difference corresponds to a 1.5% effect compared to the average brightness temperature of Venus. We have

examined the glish scripts that are used to produce these spectra, but can find no explanation for the difference in the equations used to correct for the planet angular size.

A possible explanation for the difference in intensities measured for each of the spectral bands is that the calibration process assumes a single T_{sys} value for the *reference* spectrum for each spectral band. However the system temperature gradually increases with increasing observing frequency. At the low frequency edge of each band the system temperature is over estimated and at the high frequency edge the system temperature is under estimated. Correcting for this effect would reduce the discrepancies in the overlapping frequency ranges. This model system temperature correction should be checked in future tests. The existing software does not easily allow implementing this correction.

4 Summary

The accurate measurement of the GBT efficiency allows precise measurement of the brightness temperature of the planets. These observations show that application of the GBT efficiency beam efficiency, η_B, and aperture efficiency, η_A, determined from observations of compact radio source 3C48 yield reasonable results when applied to observations of the planets.

If the antenna efficiency factors could be more accurately determined, then more precise measurement of the effective temperature of the planets could be made.

5 References

1. Altenhoff, W. J., Johnston, K. J., Stumpff, P., Webster, W. J. (1994), Astronomy and Astrophysics, vol. 287, no. 2, p. 641-646
2. Baars, J. W. M. (1973) IEEE Trans. Antennas Propagat. AP-21, no 4. 461.
3. Briggs, F. H. and Sackett, P. D. (1989), Icarus, Vol 41, 269.
4. Burns, J. O., Gisler, G. R., Borovsky, J. E., Baker, D. N., Zeilik, M. (1987), Nature, Vol 329, 234.
5. de Pater, Imke (1990), Annual Review of Astronomy and Astrophysics Vol 28, 347
6. Ghigo, F., Maddalena, R., Balser D., and Langston, G. (2001,) "GBT Commissioning Memo: Gain and Efficiency at S-band"
7. Klein, M. J. (1970), Radio Science, Vol 5, 397.
8. Ott, M. Witzel, A., Quirrenbach, A., Kirchbaum, T.P. Standke, K., J., Schalinski, C. J., and Hummel, C.A., (1994) Astronomy and Astrophysics, Vol 284 pg 331.
9. Pettengill, J. B., Ford, P. G., Chapman, B. D. 1998, J. Geophys. Res, 92(B12): 14,881-92.
10. Rao, R., Crutcher, R. M., Plambeck, R. L., and Wright, M. C. H. (1998), ApJ, 502, L75.

Start Scan	Stop Scan	Object	Scan Type	Frequency (MHz)	Elevation (d)	Start Time (UTC)
1	4	3C48	Peak	8999.999	77.4	11:05:54
5	8	3C48	Peak	8999.999	78.1	11:09:46
9	10	3C48	OffOn	8999.999	78.8	11:14:16
11	12	3C48	OffOn	8999.999	79.6	11:19:01
13	14	3C48	OffOn	8999.999	80.1	11:22:19
15	16	3C48	OffOn	9600.000	80.5	11:24:55
17	18	3C48	OffOn	9600.000	81.1	11:27:20
19	20	3C48	OffOn	8400.000	81.6	11:30:48
21	22	Mars	OffOn	8400.000	27.4	11:37:09
23	24	Mars	OffOn	8999.999	27.0	11:40:01
25	26	Mars	OffOn	9600.000	26.6	11:43:04
27	28	Venus	OffOn	8999.999	29.8	11:50:19
29	30	Venus	OffOn	8400.000	30.4	11:53:18
31	32	Venus	OffOn	9600.000	31.2	11:57:20
33	34	Venus	OffOn	8999.999	32.6	12:05:27
35	36	Venus	OffOn	8999.999	33.3	12:08:05
37	38	Venus	OffOn	8999.999	34.0	12:11:39
39	40	Saturn	OffOn	8999.999	31.6	12:14:57
41	42	Saturn	OffOn	8999.999	32.2	12:18:04
43	44	Saturn	OffOn	8999.999	33.1	12:22:49
45	46	Mercury	OffOn	8999.999	26.6	12:26:13
47	48	Mercury	OffOn	8999.999	27.1	12:28:11
49	50	Mercury	OffOn	8999.999	27.1	12:31:20
51	52	Mercury	OffOn	8999.999	27.4	12:33:17
53	54	Sun	OffOn	8999.999	27.8	12:35:18
55	56	Venus	OffOn	8999.999	38.9	12:37:41
57	58	Venus	OffOn	8999.999	39.5	12:39:46
59	60	3C48	OffOn	8999.999	79.6	12:47:41
84	85	Venus	OffOn	8999.834	46.7	13:17:12

Table 1: Scan Summary of X band observations on 2003 July 5. This observing summary was produced using the `validator` program.

Planet Name	Diameter (km)	Distance (km)	Angular Size arc-min	Angular Area arc-min^2	Elevation (d)
Mercury	4866	1.988×10^8	0.0841	5.561×10^{-3}	27.1
Mars	6760	8.015×10^7	0.2899	6.603×10^{-2}	27.0
Venus	12106	2.517×10^8	0.1653	2.147×10^{-2}	32.6
Saturn	116438	1.501×10^9	0.2667	5.586×01^{-2}	32.2

Table 2: Parameters of the Planets used for calculation of the apparent brightness of the planets, including angular size and areas on the day of observation.

Object Name	$T_{R,A}$ (K)	$T_{L,A}$ (K)	T_A (K)	Dilution Factor	Disk Factor	τ Factor	$T_B \times \eta_B$
(1)	(2)	(3)	(4)	(5)	(6)	(7)	(8)
Mercury	0.773±0.048	0.413±0.044	0.59±0.18	404.4	1.001	1.022	245 ±74
Mars	5.371±0.010	5.529±0.011	5.447±0.075	34.02	1.015	1.022	192.2 ±2.6
Venus	5.194±0.017	5.318±0.018	5.256±0.062	104.8	1.005	1.019	565 ±12
Saturn	3.216±0.020	3.181±0.015	3.198±0.035	40.27	1.012	1.019	132.1 ±1.5

Table 3: Measured antenna temperatures and computed factors. Column 8 is the brightness temperature of the planet, excluding the antenna beam efficiency factor, computed from the product of columns 4, 5, 6, and 7.

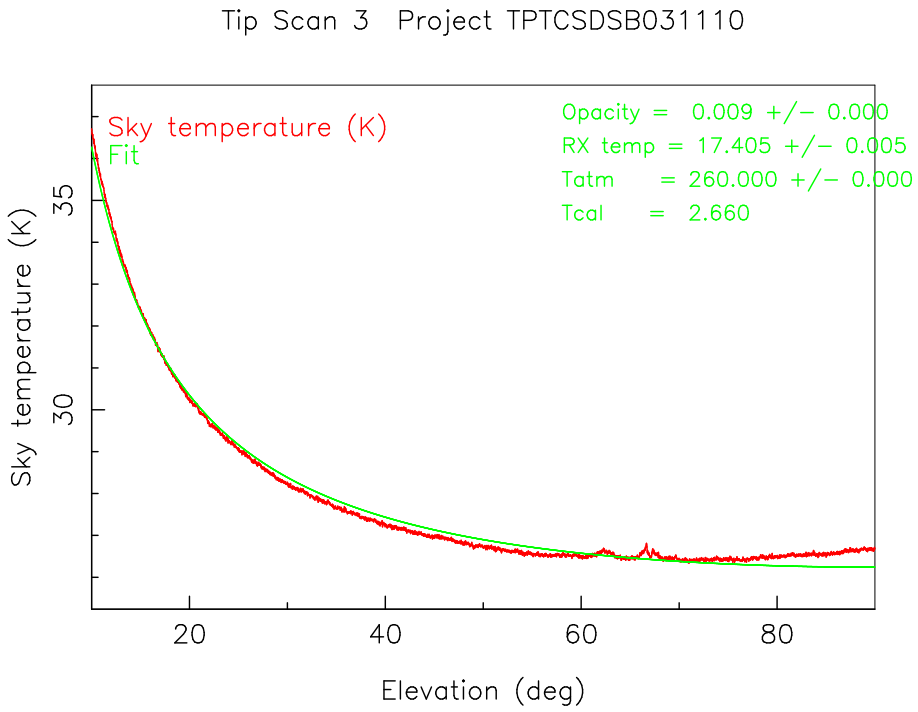

Figure 1: Tipping observations at 9.0 GHz fit to a secant(z) opacity model, where $T_{atmosphere} = 260$ is assumed.

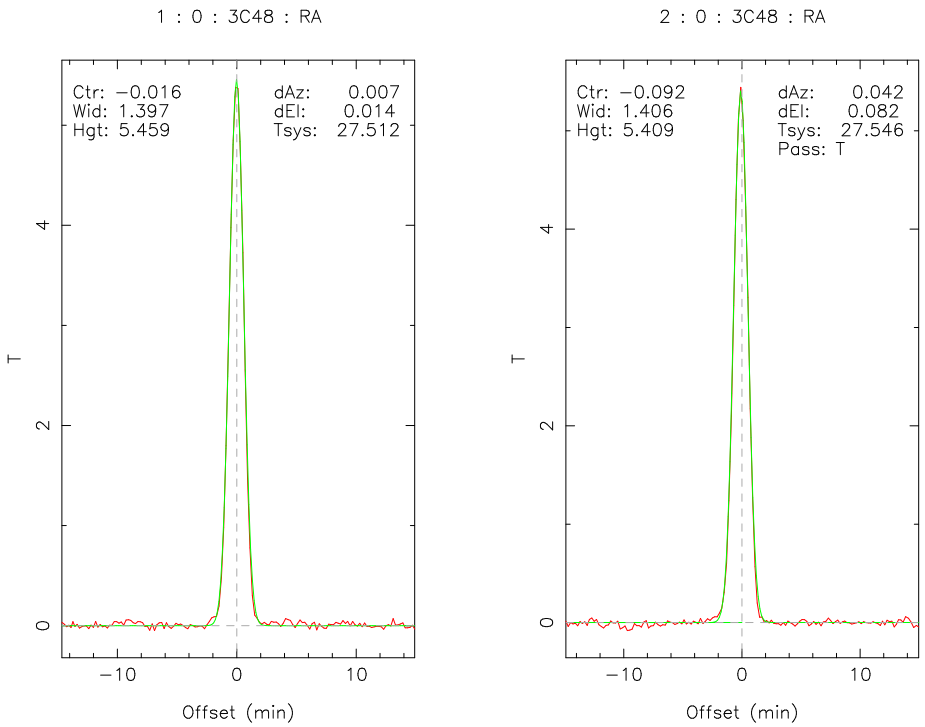

Figure 2: Pair of Peak scans in the RA direction towards 3C48.

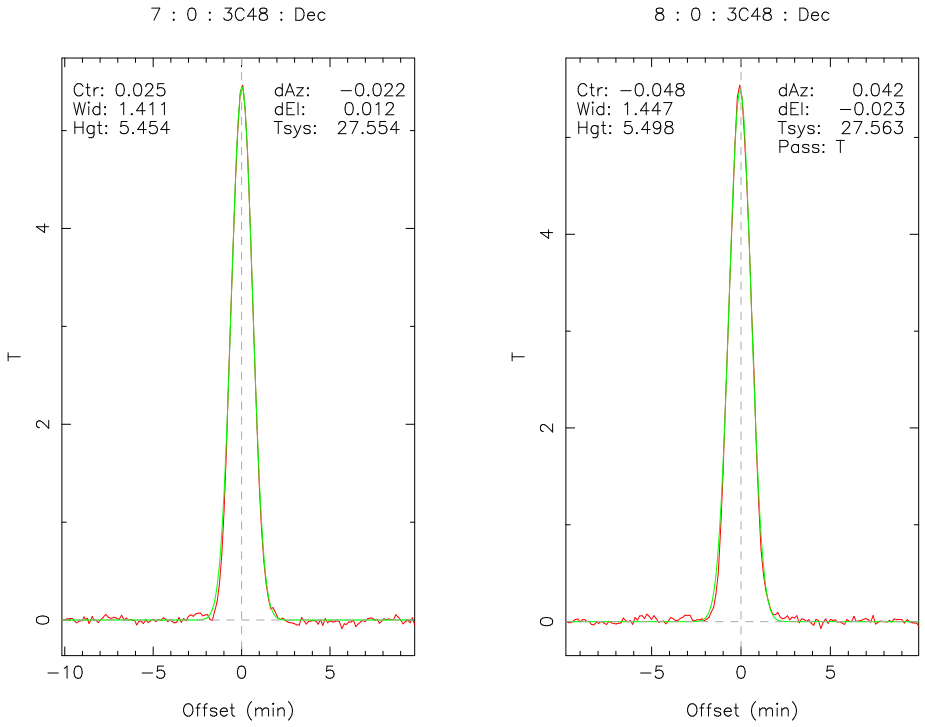

Figure 3: Pair of Peak scans in the Dec direction twoards 3C48.

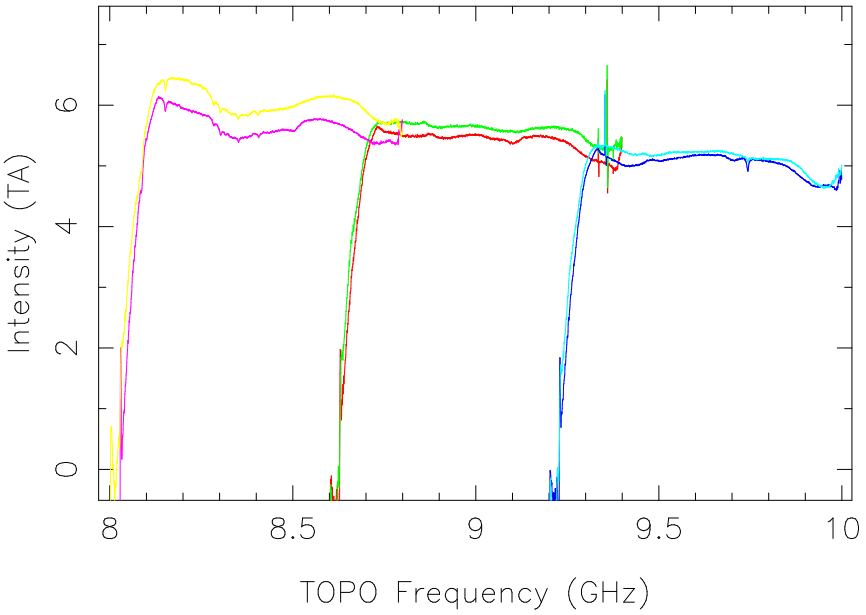

Figure 4: Antenna Temperature versus frequency plot for three pairs of OffOn scans towards calibration source 3C48. The antenna temperature is calibrated by measurement of the calibration noise diode intensity, which is toggled on and off at a 1 Hz rate during the observations.

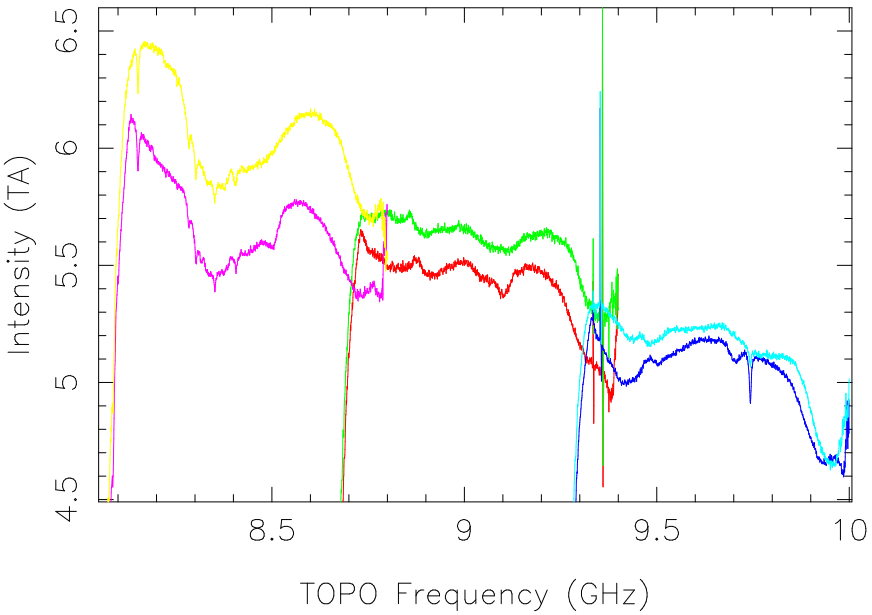

Figure 5: Antenna Temperature versus frequency plot for three pairs of OffOn scans towards calibration source 3C48. Same as previous figure except the temperature range is centered on the average 3C48 temperature. Although the radio spectrum of 3C48 is expected to be very smooth, a number of narrow features are seen in the spectrum. These features are due to properties of the feed and receiver system.

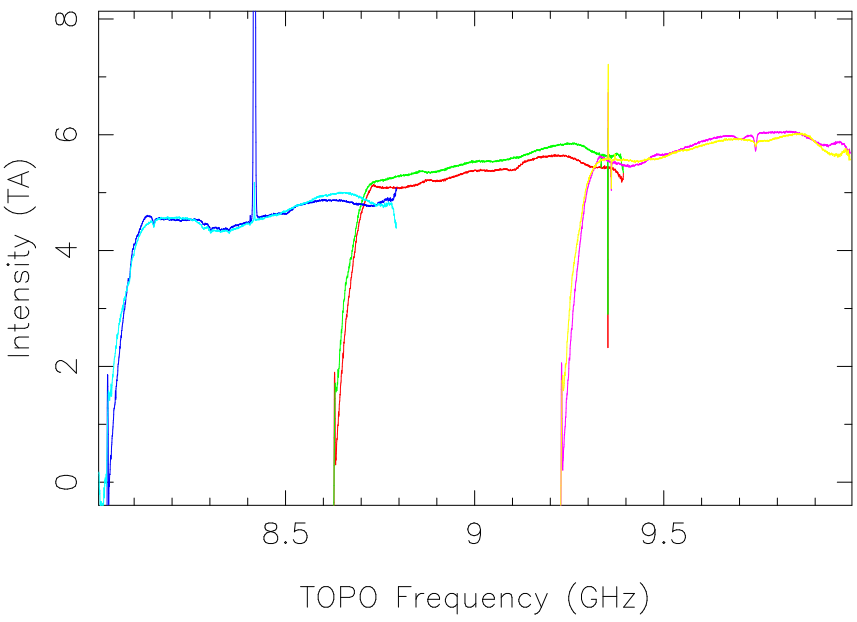

Figure 6: Antenna Temperature versus frequency plot for three pairs of OffOn scans towards planet Mars. The antenna temperature is calibrated by measurement of the calibration noise diode intensity, which is toggled on and off at a 1 Hz rate during the observations.

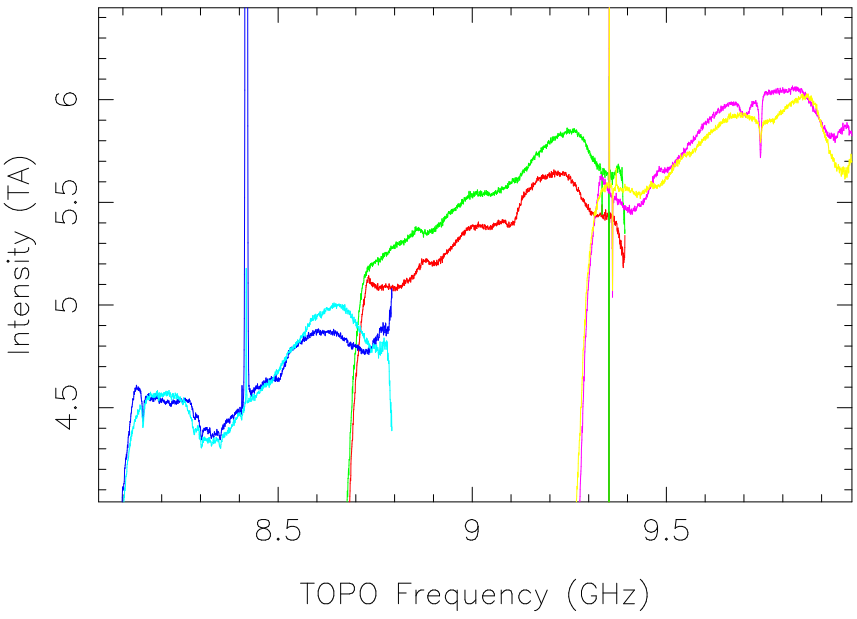

Figure 7: Antenna Temperature versus frequency plot for three pairs of OffOn scans towards planet Mars. Same as previous figure except the temperature range is centered on the average Mars temperature. Although the radio spectrum of Mars is expected to be very smooth, a number of narrow features are seen in the spectrum. These features are due to properties of the feed and receiver system.

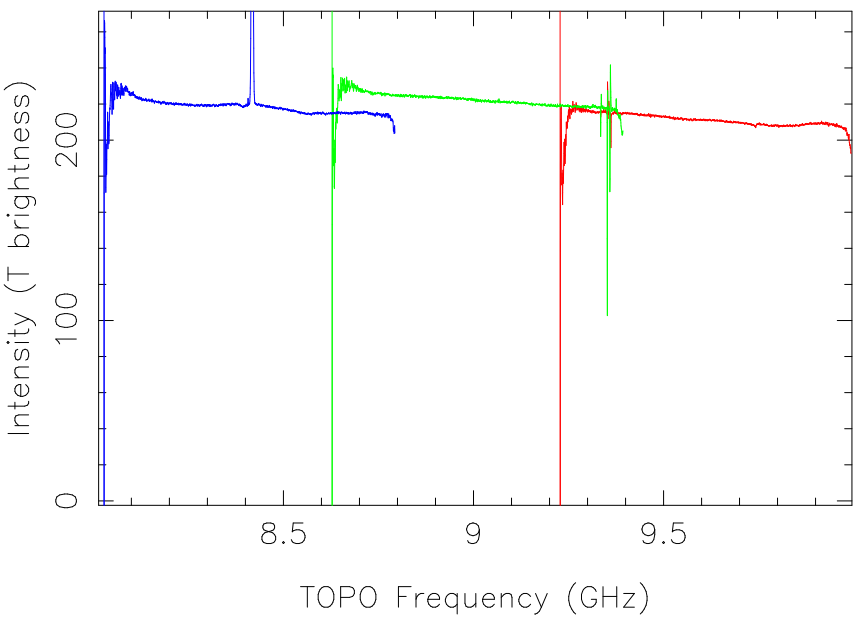

Figure 8: Brightness Temperature versus frequency plot for three pairs of OffOn scans towards planet Mars. The antenna temperature is converted to brightness temperature by the application of measurements of source 3C48, described in the text.

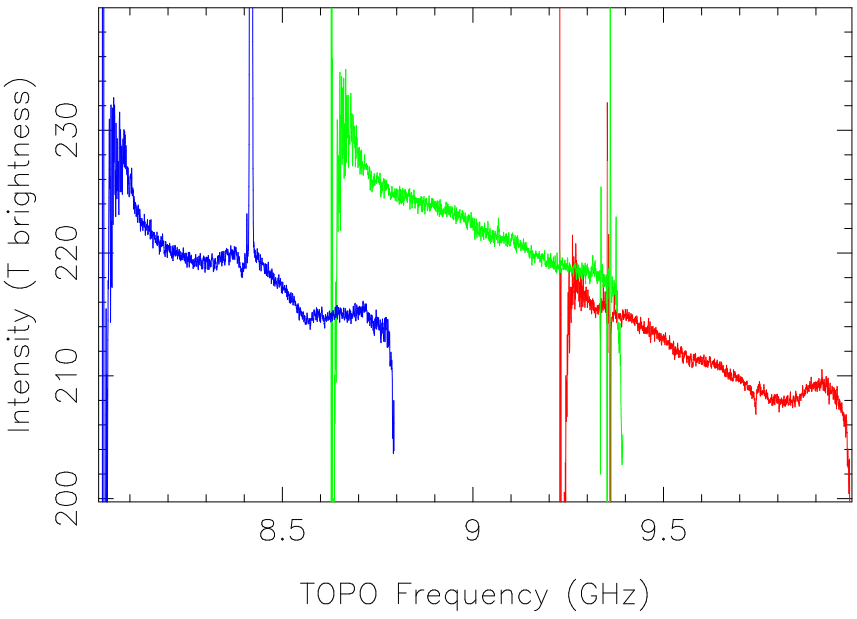

Figure 9: Brightness Temperature versus frequency plot for three pairs of OffOn scans towards planet Mars. Same as previous figure except the temperature range is centered on the average Mars temperature. Notice this calibration process removes the sharp features in the Mars spectrum due to the GBT feed and receiver system.

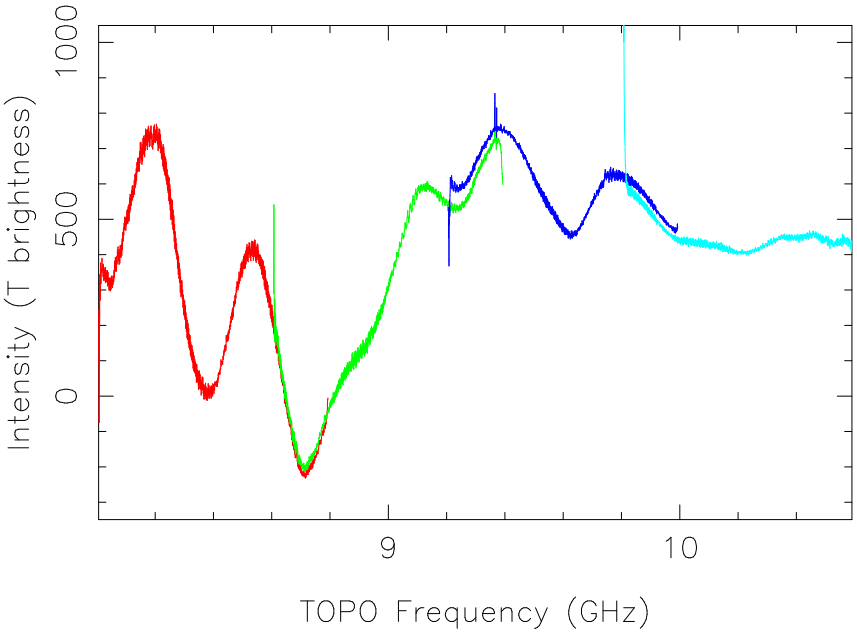

Figure 10: Brightness Temperature versus frequency plot in 4 spectral bands for planet Mercury. The undulations in the spectrum are due to sidelobes of the Sun.

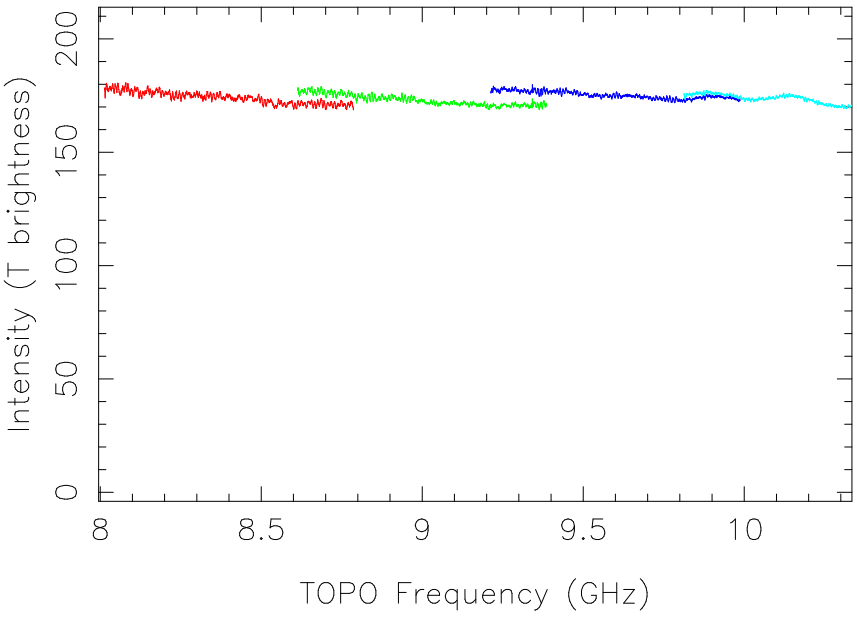

Figure 11: Brightness Temperature versus frequency plot in 4 spectral bands for planet Saturn. The high frequency undulations in the spectrum are due to effects of the Sun in the sidelobes.

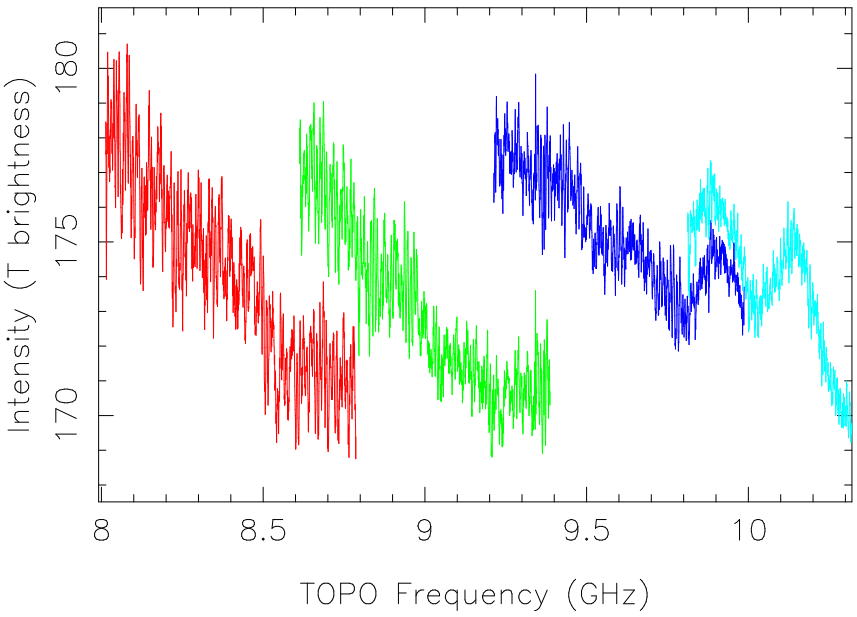

Figure 12: Brightness Temperature versus frequency plot in 4 spectral bans for planet Saturn. Same as previous figure, centered on the average brightness temperature of the planet.

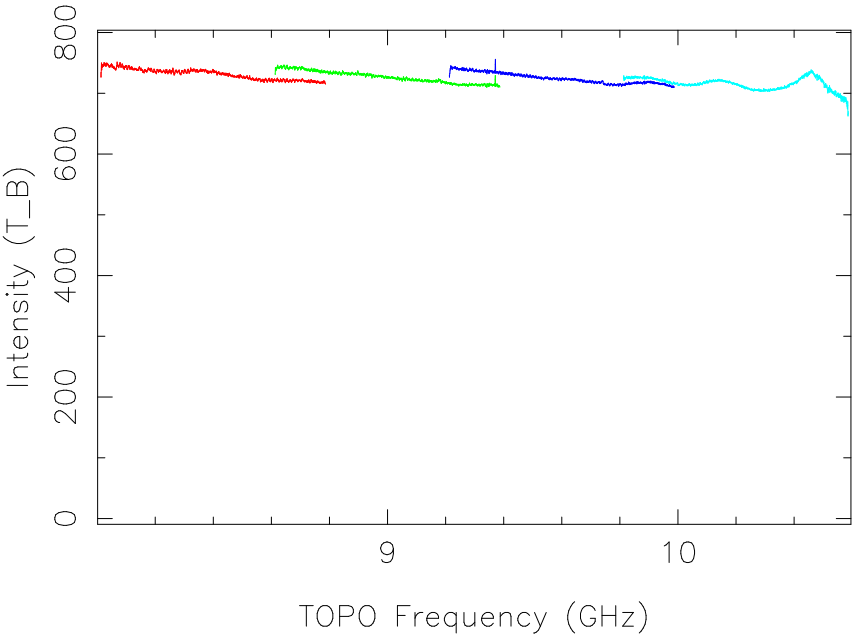

Figure 13: Brightness Temperature versus frequency plot in 4 spectral bands for planet Venus. The high frequency undulations in the spectrum are due to effects of the Sun in the sidelobes.

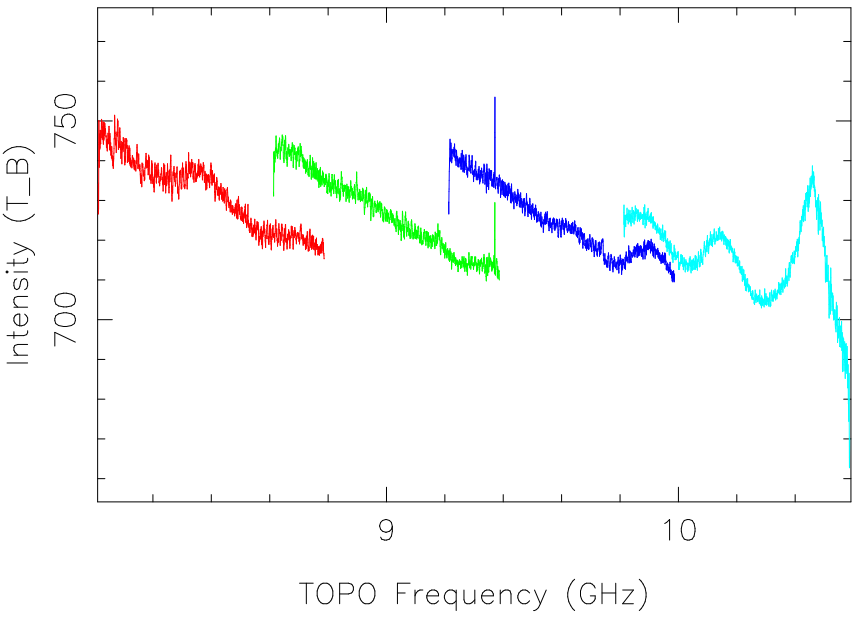

Figure 14: Brightness Temperature versus frequency plot in 4 spectral bans for planet Venus. Same as previous figure, centered on the average brightness temperature of the planet.

A Glish Script: marsTemp.g

Glish scripts are used to generate the physical temperature plots for the planets based on observations of calibration sources (glish scripts for calibration of these observations are available on-line at http://www.gb.nrao.edu/~glangsto/gbt/x). An example Glish script is shown below:

```
#script to calculate brightness temperature of Mars as function of frequency
#HISTORY
# 040302 GIL clean up comments
# 040301 GIL attempt correction of \eta_B
# 040226 GIL update constants
# 040217 GIL re-order and compute Temp for 3 frequency bands
# 040212 GIL fix glish errors
# 040202 GIL change in filler from SPECTROEMTER TO ACS
# 031010 GIL add comments, make function physicalTemp()
# 030801 GIL initial version for summer school

# The observations were performed at C band, with 4 banks of 800 MHz each
scanCal := 13     # scan for calibration  (3C48 @ 9 GHz)
scanSrc := 25     # scan with source      (Mars @ 9 GHz)

dataName := '/home/archive/test-data/tape-0001/TSDSS_01'

print 'About to import data....'
d.import( dataName,,,scanCal,scanSrc+1);
c := 299792458                  # speed of light in m/sec
k := 1.38 * 10^-23              # boltzman's constant

# utilities needed to do the calculations
include '/users/glangsto/flareGlish/ott.g'
include '/users/glangsto/flareGlish/polAvg.g'
include '/users/glangsto/flareGlish/reduce1B.g'

#              diameter                    orbital radius
SunKm       :=  1391900 ; SunOrbitKm    :=   1391900
MercuryKm   :=  4866 ; MercuryOrbitKm   :=  57950000  ;
VenusKm  := 12106 ; VenusOrbitKm  := 108110000  ;
EarthKm  := 12742 ; EarthOrbitKm  := 149570000  ;
MarsKm      :=  6760 ; MarsOrbitKm      :=  227840000  ;
JupiterKm  := 139516; JupiterOrbitKm  :=  778140000  ;
SaturnKm  := 116438; SaturnOrbitKm  := 1427000000  ;
UranusKm  := 46940 ; UranusOrbitKm  := 2870300000  ;
NeptuneKm  := 45432 ; NeptuneOrbitKm  := 4499900000  ;
PlutoKm  :=  2274 ; PlutoOrbitKm  := 5913000000  ;

#distances to the planets on this day; from orbitPlanet
#                   seconds
#03JUL05 16h00m00   663.066   6h59m20  24d07'03" Mercury
#03JUL05 16h00m00   839.672   6h04m58  23d21'54" Venus
#03JUL05 16h00m00     1.256  11h50m47   5d46'20" Moon
#03JUL05 16h00m00   267.351  22h40m28 -13d20'44" Mars
#03JUL05 16h00m00  3070.178   9h26m08  15d56'04" Jupiter
#03JUL05 16h00m00  5006.668   6h17m41  22d35'24" Saturn
#03JUL05 16h00m00  9655.915  22h19m03 -11d18'23" Uranus
#03JUL05 16h00m00 14566.165  21h00m04 -17d01'56" Neptune
#03JUL05 16h00m00 14848.257  17h11m04 -13d28'15" Pluto

diameterKm := MarsKm            #diameter of mars (km)
```

```
distanceS  := 267.351            #distance to mars (seconds)
distanceKm := distanceS * c/1000.#distance to planet (km)

#get calibration source parameters
calSdRec := polAvg( d.getscan(scanCal))
d.plotscan(calSdRec)                    # now examine
calTemps    := getData(calSdRec)          # vector arrays end in 's'
calFreqs    := getFreq(calSdRec)
nChannels   := length( calTemps);
centerFreq  := calFreqs[nChannels/2]   # get center freq MHz
centerLambda := c/(10000.*centerFreq)  # wavelength in cm
tau         := 0.01                    # atmospheric attenuation
etaR        := 0.99                    # radiation efficiency
Km          := 0.000171539002          # conversion factor for main beam size
                                       # Ie: OmegaM = Km * (lambda/m)^2
Ag          := 7854                    # Geometric area of the GBT (m^2)

#function to show the scale parameters for physical temp calculations
showFactors := function (centerLambda,  diameterKm, distanceKm, srcEl) {
  global x, K, omegaM, thetaS, srcArea, thetaSArcMin

  thetaS       := diameterKm/distanceKm  # angular size (radians)
  thetaSArcMin := thetaS * ((180*60)/pi)
  srcArea := thetaS*thetaS * pi/4.       # angular area of planet (sr)

  thetaArcMin := 0.423 * centerLambda    # gbt FWHM in arcmin
  thetaA      := thetaArcMin / ((180*60)/pi)   # angle in radians
  print ''

  x           := thetaS / (1.2 * thetaA) # baars 1973 eq. 12.
  K           := x*x / ( 1- exp( -x*x))  # baars 1973 eq. 12

  print 'For  wavelength      = ', centerLambda, ' cm '
  print 'For  frequency       = ', 29.97/centerLambda, ' MHz'
  print 'Beam FWHM            = ', thetaArcMin, 'Arc Min'
  print 'Src  Size            = ', thetaSArcMin, 'Arc Min'
  omegaM      := 1.133 * thetaA * thetaA

  print 'Dilution Factor      = ', omegaM/ srcArea
  print 'Disk     Factor      = ', K

  print 'Assuming atmospheric attenuation = ', tau, ' tau at El = ',srcEl,' d'
  print '         atmospheric correction  = ', exp( tau/sin(srcEl*pi/180.))
  print ''
  return T;
} # end of showFactors()

showFactors( centerLambda, diameterKm, distanceKm, srcEl=27)

#function to convert source antenna temp to brightness Temperature
physicalTemp := function( scanCal, scanSrc, srcArea)
{ # for debugging, make variables global
  global calSdRec, srcSdRec, srcSdRecPhysTemp, sd, srcTemps, etaBs
  global xs, Ks, thetaAs, tauFactor, srcEl, omegaBs, calFluxs, calTemps
  global lambdas

  calSdRec2 := reduceSR( scanCal+1, scanCal)  # Calibrate cal (Assume OffOn
```

```
  # produce a polarization average Single dish record
  calSdRec := polAvg( calSdRec2)
  d.plotscan(calSdRec)                  # now examine
  calTemps := getData(calSdRec)         # vector arrays end in 's'
  calFreqs := getFreq(calSdRec)
  nChannels := length( calTemps);
  endChannels := nChannels/128

  # get the calibration source name
  calSourceName := calSdRec.other.gbt_go.OBJECT
  calFluxs := ottFlux(calSourceName, calFreqs)
  calEl    := calSdRec.header.azel.m1.value
  lambdas  := (c*10^-6)/calFreqs                  # convert freq (MHz) to m

  thetaAs  := 0.423 * lambdas * 100. / (180*60/pi) # angle in radians
  omegaBs  := 1.133*thetaAs*thetaAs                # beam areas
  xs       := thetaS / (1.2 * thetaAs)   # baars 1973 eq. 12.
  #factor to correct observed temperature for a disk shaped source
  Ks       := xs*xs / ( 1- exp( -xs*xs))  # baars 1973 eq. 12

  srcSdRec2 := reduceTP( (scanSrc+1), scanSrc)
  srcSdRec := polAvg( srcSdRec2)
  srcEl    := srcSdRec.header.azel.m1.value
  d.plotscan( srcSdRec)

  # now get source temps and convert to flux density
  srcTemps  := getData(srcSdRec)

  #the tau factor is the difference in attenuation of source and calibrator
  tauFactor := exp( tau/sin(srcEl)) * exp( -tau/sin(calEl))

  print 'Tau Factor           = ', tauFactor,' :=', exp( tau/sin(srcEl)),' / ', exp( tau/sin(calEl))

  etaAs := calTemps/(2.845 * calFluxs)
  etaBs := (etaAs * omegaBs * Ag )/ ( etaR * lambdas * lambdas)
  srcPhysTemps := (tauFactor*Ks*(omegaBs/srcArea)*srcTemps)/etaBs

  srcSdRecPhysTemp := putData( srcSdRec, srcPhysTemps)
  srcSdRecPhysTemp.data.desc.units := 'T brightness'
  d.plotscan( srcSdRecPhysTemp)

  return (srcSdRecPhysTemp);
} # end of physicalTemp()

d.open('TSDSS_01_ACS')
#compute the physical temperatures for the planet
marsSdRec9000 := physicalTemp ( 13, 23, srcArea)
marsSdRec8400 := physicalTemp ( 19, 21, srcArea)
marsSdRec9600 := physicalTemp ( 17, 25, srcArea)
#plot all scans; turn plotter overlay on!
d.plotscan(marsSdRec8400);d.plotscan(marsSdRec9000);d.plotscan(marsSdRec9600)
```